THE JOURNAL OF PHYSICAL CHEMISTRY B
A JOURNAL OF THE AMERICAN CHEMICAL SOCIETY

pubs.acs.org/JPCB

Article

Computational Design and Experimental Validation of ACE2-Derived Peptides as SARS-CoV-2 Receptor Binding Domain Inhibitors

Published as part of The Journal of Physical Chemistry virtual special issue "Pablo G. Debenedetti Festschrift".

Sudeep Sarma,[#] Stephanie M. Herrera,[#] Xingqing Xiao, Gregory A. Hudalla, and Carol K. Hall*

Cite This: *J. Phys. Chem. B* 2022, 126, 8129–8139

Read Online

ACCESS | Metrics & More | Article Recommendations | Supporting Information

ABSTRACT: The COVID-19 pandemic has caused significant social and economic disruption across the globe. Cellular entry of SARS-CoV-2 into the human body is mediated via binding of the Receptor Binding Domain (RBD) on the viral Spike protein (SARS-CoV-2 RBD) to Angiotensin-Converting Enzyme 2 (ACE2) expressed on host cells. Molecules that can disrupt ACE2:RBD interactions are attractive therapeutic candidates to prevent virus entry into human cells. A computational strategy that combines our Peptide Binding Design (PepBD) algorithm with atomistic molecular dynamics simulations was used to design new inhibitory peptide candidates via sequence iteration starting with a 23-mer peptide, referred to as SBP1. SBP1 is derived from a region of the ACE2 Peptidase Domain α1 helix that binds to the SARS-CoV-2 RBD of the initial Wuhan-Hu-1 strain. Three peptides demonstrated a solution-phase RBD-binding dissociation constant in the micromolar range during tryptophan fluorescence quenching experiments, one peptide did not bind, and one was insoluble at micromolar concentrations. However, in competitive ELISA assays, none of these peptides could outcompete ACE2 binding to SARS-CoV-2-RBD up to concentrations of 50 μM, similar to the parent SBP1 peptide which also failed to outcompete ACE2:RBD binding. Molecular dynamics simulations suggest that P4 would have a good binding affinity for the RBD domain of Beta-B.1.351, Gamma-P.1, Kappa-B.1.617.1, Delta-B.1.617.2, and Omicron-B.1.1.529 variants, but not the Alpha variant. Consistent with this, P4 bound Kappa-B.1.617.1 and Delta-B.1.617.2 RBD with micromolar affinity in tryptophan fluorescence quenching experiments. Collectively, these data show that while relatively short unstructured peptides can bind to SARS-CoV-2 RBD with moderate affinity, they are incapable of outcompeting the strong interactions between RBD and ACE2.

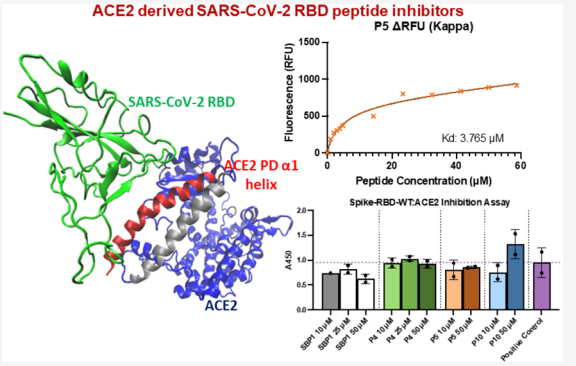

1. INTRODUCTION

Since the first report by the World Health Organization in December 2019, severe acute respiratory syndrome coronavirus 2 (SARS-CoV-2) has heavily impacted the global community. As of November 2021, there have been more than 250 million confirmed cases of COVID-19 globally, resulting in more than 5 million deaths.[1] The advent of vaccines at the end of 2020 and government-supported vaccination campaigns have reduced the infection rate. However, a slow rollout of vaccines in conjunction with the emergence of more contagious variants of SARS-CoV-2, such as lineages B.1.1.7 (Alpha variant), B.1.351 (Beta variant), P.1 (Gamma variant), B.1.617.1 (Kappa variant), B.1.617.2 (Delta variant), and B.1.1.529 (Omicron variant),[2,3] have further prolonged the severity of this pandemic. As the pandemic continues to evolve, so too does the need to develop effective therapeutics capable of reducing infection rate, transmission, hospitalizations, and recovery time for infected patients.

The initial Wuhan-Hu-1 strain of SARS-CoV-2 has been shown to share an 86.9% sequence identity with SARS-CoV, a coronavirus that emerged in 2002−2004, and both viruses rely on the same human host receptor, Angiotensin-Converting Enzyme II (ACE2), for cell entry.[4,5] (Hereafter, we refer to this initial strain of SARS-CoV-2 as a Wild-type (WT) strain.) ACE2 is expressed on the surface of human cell membranes where it facilitates the maturation of angiotensin. Entry of SARS-CoV-2 into host cells is mediated by its Spike viral protein, which can bind to ACE2 and subsequently initiate membrane fusion between the virus and host cells. The Spike protein has 1273 amino acids and contains two subunits, S1

Received: June 6, 2022
Revised: September 28, 2022
Published: October 11, 2022

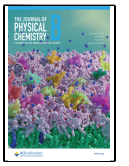

https://doi.org/10.1021/acs.jpcb.2c03918
J. Phys. Chem. B 2022, 126, 8129−8139

and S2, which are present on the viral membrane and protrude outward, having a "corona-like" appearance. The Spike protein subunit S1 binds to the peptidase domain (PD) of ACE2 via its Receptor Binding Domain (RBD), while subunit S2 mediates membrane fusion. The recognition of ACE2 by SARS-CoV-2 involves direct interactions between the RBD pocket and the α1 and α2 helices of the ACE2 PD. The affinity between SARS-CoV-2 WT and ACE2, measured by Wrapp et al. using surface plasmon resonance, was found to be $K_d \sim 15$ nM.[6−8]

Peptide sequences derived from ACE2 can competitively inhibit the interaction between SARS-CoV-2 Spike protein and ACE2 that is required for viral infection of host cells. Chan et al. developed high-affinity decoy receptors through a deep mutagenesis approach that identified amino acid substitutions within ACE2 that increased Spike binding.[9] Separate computational and experimental studies reported ACE2-derived α-helical peptides that bound to the RBD WT and exhibited modest antiviral activity, respectively.[10,11] The Pentelute lab synthesized a 23-mer peptide (sequence: *IEEQAK***TFLDKFNHEAED***LFYQS*) termed "SBP1", derived from the ACE2 PD α1 helix (residue numbers: 21−43); its binding activity to the SARS-CoV-2 RBD WT was observed to be ∼1.3 μM using biolayer interferometry (BLI).[12,13] Notably, a shorter 12-mer peptide derived from SBP1 (sequence: **TFLDKFNHEAED**, residue numbers: 27−38 on the ACE2 PD α1 helix), termed "SBP2", was not observed to bind to RBD. The same group also screened a library of peptide candidates against the RBD using high-affinity selection mass-spectrometry; however, the identified consensus peptide did not compete for ACE2 binding. It was instead predicted to bind at a different site on RBD than ACE2, highlighting the importance of the binding pocket on SARS-CoV-2 RBD for the design of effective competitive binding inhibitors.[14]

Examining the interfacial interactions between the Spike-RBD and ACE2 α1 helix may enable the discovery of new peptide-based competitive inhibitors. An ideal inhibitor should resemble SBP1 but exhibit a stronger affinity for the SARS-CoV-2 RBD than ACE2. To increase the binding affinity of the SBP1-mimicking peptides for SARS-CoV-2 RBD, we employed PepBD, an automated peptide binding design algorithm developed in the Hall group, to redesign the central portion of SBP1 ("SBP2", residue numbers: 27−38) while keeping the flanking sequences at the SBP1 N-/C-terminus (residue numbers: 21−26 and 39−43) fixed. Thus, within the general SBP1 sequence, *IEEQAK*$\mathbf{X_1X_2X_3X_4X_5X_6X_7X_8X_9X_{10}X_{11}X_{12}}$*LFYQS*, PepBD iterates the amino acids in each of the X_i (i = 1−12) positions to generate a large library of variants that are then analyzed in silico for their RBD-WT binding affinity. The PepBD algorithm uses atomistic force fields, rather than knowledge-based information, which to date has enabled the discovery of high-affinity binding peptides to targets that have no known binders available in the protein data bank.[15−19] For example, the PepBD algorithm has been used to design 15-mer $tRNA^{Lys3}$-binding peptides for the inhibition of HIV reverse transcriptase,[15−21] 12-mer peptide-based biological recognition elements for cardiac troponin I[22] and for neuropeptide Y to detect human performance indicators,[23] Protein-A mimetic peptide ligands to bind to immunoglobulin G for monoclonal antibody purification,[24] peptide ligands that bind to the Fab fragment of immunoglobulin G,[25] and peptide inhibitors targeting *C. diff.* toxins to neutralize the cytopathic effects of the toxins.[26]

Highlights of our results are as follows. The PepBD algorithm sampled approximately 450000 different peptide sequences from a pool of $\sim 10^{13}$ possible peptide candidates. Lead compounds from our computational search were subjected to explicit-solvent atomistic MD simulations. The implicit-solvent molecular mechanics/generalized Born surface area (MM/GBSA) approach with the variable internal dielectric constant model was used to estimate binding free energies. We report 10 peptides that have a higher binding affinity for SARS-CoV-2 RBD WT than SBP1 based on our in silico analyses. Five peptides with favorable predicted binding free energies were synthesized using conventional solid-phase peptide synthesis methods. Of these, four of the peptides were soluble in water up to mM concentrations. These four peptides were tested for RBD-WT binding using a solution-phase tryptophan fluorescence quenching binding assay that avoids immobilization of either receptor or ligand. Competitive inhibition of ACE2:SARS-CoV-2 RBD WT interactions by these peptides was measured with an enzyme-linked immunosorbent assay (ELISA). Three of the four peptides bound RBD with micromolar solution-phase affinity, but none of the three were capable of inhibiting ACE2:SARS-CoV-2 RBD WT interactions in the ELISA assay. Likewise, SBP1 failed to inhibit ACE2:SARS-CoV-2 RBD WT interactions in the ELISA assay. Additional molecular dynamics simulations of peptides SBP1 and P4 bound to the RBD of the Alpha, Beta, Gamma, Kappa, Delta, and Omicron variants suggest that P4 binds with higher affinity than SBP1 to all variants except the Alpha variant. Tryptophan fluorescence quenching assays demonstrated that P4 bound to the SARS-CoV-2 RBD of Kappa-B.1.617.1 and Delta-B.1.617.2 with micromolar affinity, supporting these predictions. Collectively, these data demonstrate the potential to design peptides that recognize the broad spectrum of SARS-CoV-2 RBD variants using the PepBD algorithm for the development of SARS-CoV-2 diagnostics and drug-delivery applications.

2. MATERIALS AND METHODS

2.1. Computational Peptide Design Algorithm. The PepBD algorithm uses an iterative procedure that optimizes peptide sequences to bind with higher affinity and specificity to a biomolecular target than a known reference ligand. The algorithm requires a starting input structure for the complex formed by an initial peptide sequence (reference ligand) and the biomolecular target. This can be obtained from the PDB, standard docking algorithms, crystallography, NMR, or from atomistic molecular dynamics simulations. The design algorithm performs 10,000 evolution steps and generates variants to the original peptide that bind to the target protein by two kinds of moves: sequence change and conformation change. Each step samples approximately 20 different peptide sequences or conformations. If a sequence change move is selected, two kinds of trials that move to change the peptide sequence are considered: (1) random substitution of a new residue for an old one of the same residue type and (2) exchange of amino acids at two random sites on the peptide. The 20 natural amino acids are classified into six residue types according to their hydrophobicity, polarity, charge, and size (see Supporting Information, Table S1). If a conformation change move is selected, a random number is generated to decide which of three possible types of changes to the peptide backbone conformation will be made: (1) concerted rotation (CONROT) to displace three consecutive residues in the

https://doi.org/10.1021/acs.jpcb.2c03918
J. Phys. Chem. B 2022, 126, 8129−8139

middle of the peptide chain leaving the outermost residues fixed, (2) rotation of the N- or C-terminus plus two residues in the middle, and (3) rotation of the entire peptide backbone. Energy minimization is conducted to determine optimal side chain configurations of the amino acids, allowing the trial peptide chains to be repacked fully without atomic overlaps. The score of the newly generated peptide sequence or conformer is evaluated and the Monte Carlo Metropolis algorithm is used to accept or reject the new trial peptide. More details regarding the PepBD algorithm can be found in our previous work.[15−20]

The score function that we use to evaluate newly generated peptide candidates is given by

$$\Gamma_{\text{score}} = \Delta E_{\text{binding}} + \lambda(E^{\text{bound}}_{\text{peptide-VDW}} + E^{\text{bound}}_{\text{peptide-ELE}} + E^{\text{bound}}_{\text{peptide-EGB}}) \quad (1)$$

The first term of eq 1, $\Delta E_{\text{binding}}$, accounts for the difference in the energy of the complex and the energies of the peptide and target biomolecule prior to binding. This requires calculation of the internal energy, van der Waals energy (VDW), electrostatic energy (ELE), and polar solvation energy (EGB). The second term is the peptide stability term and accounts for the energy of the free peptide in the bound-state configuration. It is the sum of the van der Waals energy (VDW), electrostatic energy (ELE), and polar solvation energy (EGB) of the peptide prior to binding. Lower scores mean better binders. The force field parameters are taken from the Amber 14SB force field.

2.2. Explicit-Solvent Atomistic Molecular Dynamics Simulation. Explicit-solvent atomistic MD simulations are carried out in the canonical (NVT) ensemble using the AMBER 18 package to examine the dynamics of the binding process between the starting peptide sequence, SBP1 (hACE2 amino acids 21−43), and the best-scoring evolved peptides (viz. peptides discovered via the algorithm) to the SARS-CoV-2 RBD. The starting conformations of the SARS-CoV-2 RBD and the best-scoring peptide complexes for the atomistic MD simulations are obtained from our peptide search algorithm. Three independent simulations are carried out for each peptide:SARS-CoV-2 RBD complex for 100 ns to ensure that the system reaches an equilibrated state. Each peptide−receptor complex is solvated in a periodically truncated octahedral box containing a 12 Å buffer of TIP3P water (∼14000 water molecules) surrounding the complex in each direction. Particle Mesh Ewald (PME) summation is used to calculate the long-ranged electrostatic interactions with a cutoff radius of 8 Å and a 1×10^{-5} tolerance for the Ewald convergence to calculate the nonbonded interactions. Hierarchical clustering analysis is performed on the last 5 ns of the simulation trajectories to obtain the representative structure of the complexes in solution. The implicit-solvent molecular mechanics/generalized Born surface area (MM/GBSA) approach with the variable internal dielectric constant model is used to post-analyze the last 5 ns simulation trajectories of the peptide:SARS-CoV-2 RBD complexes to calculate the binding free energies. Details of the computational procedures and post-analysis of the atomistic MD simulations can be found in our previous work.[15−20]

2.3. In Vitro Peptide Preparation. Peptides were synthesized and purified to (≥95%) by GenScript Biotech Corporation (Piscataway, NJ, U.S.A.). Due to their negative charge, lyophilized peptides were dissolved in 5% (v/v) NH_4OH in ultrapure deionized water. The molar concentration of reconstituted peptides was measured using a NanoDrop spectrophotometer (ThermoFisher; λ = 280 nm). For fluorescence quenching experiments, reconstituted peptides were diluted 1:1 (v/v) in 2× phosphate buffered saline (PBS; 274 mM NaCl, 5.4 mM KCl, 20 mM Na_2HPO_4 and 3.2 mM KH_2PO_4, pH 7.4). For competitive inhibition ELISA assays, reconstituted peptides were diluted in 0.5 M DMSO in H_2O to a final concentration of 50, 75, or 100 μM. These concentrations were used to create a peptide range from 0.01 to 100 μM.

2.4. Tryptophan Fluorescence Quenching of SARS-CoV-2 RBD by PepBD Designed Peptides. SARS-CoV-2 (2019-nCoV) SARS-CoV-2 RBD-His Recombinant Protein (Sino Biological, Baculovirus-Insect Cells Derived, 40592-V08B), κ SARS-CoV-2 (2019-nCoV), SARS-CoV-2 RBD Protein (Sino Biological, HEK293 Cells Derived, 40592-V08H88), and δ SARS-CoV-2 RBD Protein (Sino Biological, HEK293 Cells Derived, 40592-V08H115) were purchased and used as provided by the manufacturer. Tryptophan fluorescence quenching was measured using a SpectraMax M5 plate-reader in a quartz cuvette (NC9030411, ThermoFisher) by adapting previously reported methods.[27] Here, tryptophan fluorescence quenching was measured by adding six 5 μL increments of a 0.1 mM peptide stock solution followed by six 5 μL increments of 1 mM peptide stock solution to 500 μL of SARS-CoV-2 RBD (2.5 μM) in 1× PBS, with tryptophan fluorescence of the sample measured after addition of each peptide volume increment (excitation λ = 280 nm; emission λ = 335 nm). As negative controls, (1) 12 5 μL increments of ultrapure deionized water were added to 500 μL of SARS-CoV-2 RBD (2.5 μM) in 1× PBS or (2) peptide was added in six 5 μL increments of a 0.1 mM peptide stock solution, followed by six 5 μL increments of 1 mM peptide stock solution, to ultrapure deionized water, with tryptophan fluorescence of the controls measured after addition of each water or peptide volume increment (excitation λ = 280 nm; emission λ = 335 nm). All peptides designed by PepBD had at least one tryptophan residue, whereas SBP1 has no tryptophan residues. Thus, only the peptides designed by PepBD were evaluated using this method.

The change in tryptophan fluorescence (ΔRFU) relative to baseline was calculated by subtracting RFU (relative fluorescence units) of experimental samples containing protein and peptide (i.e., quenched fluorescence signal) from the sum of the RFUs of control samples containing only peptide and of control samples containing only protein, which we refer to as the "estimated RFU". Dissociation constants were estimated by nonlinear regression using GraphPad Prism software. To account for experimental variability for all experiments where ΔRFU was significantly greater than zero, three independent experiments were performed; when ΔRFU was not significantly different from baseline, only two independent experiments were performed.

2.5. ELISA-Based ACE2:SARS-CoV-2 RBD Binding Assay. The relative abilities of different peptides to competitively inhibit ACE2:SARS-CoV-2 RBD WT binding were characterized using a commercially available COVID-19 ACE2:SARS-CoV-2 RBD WT Binding Assay Kit (RayBio-Tech, CoV-ACE2S2−1) according to the manufacturer's instructions. Serial dilutions of SBP1 or PepBD-designed peptide stock solutions (0.001, 0.01, 0.1, 1, 2.5, 5, 10, 25, 50, 75, and 100 μM) were first mixed with recombinant SARS-CoV-2 RBD WT with an Fc tag at a ratio of 3:1 (v/v). These solutions were then added to wells of a 96-well plate that had

https://doi.org/10.1021/acs.jpcb.2c03918
J. Phys. Chem. B 2022, 126, 8129−8139

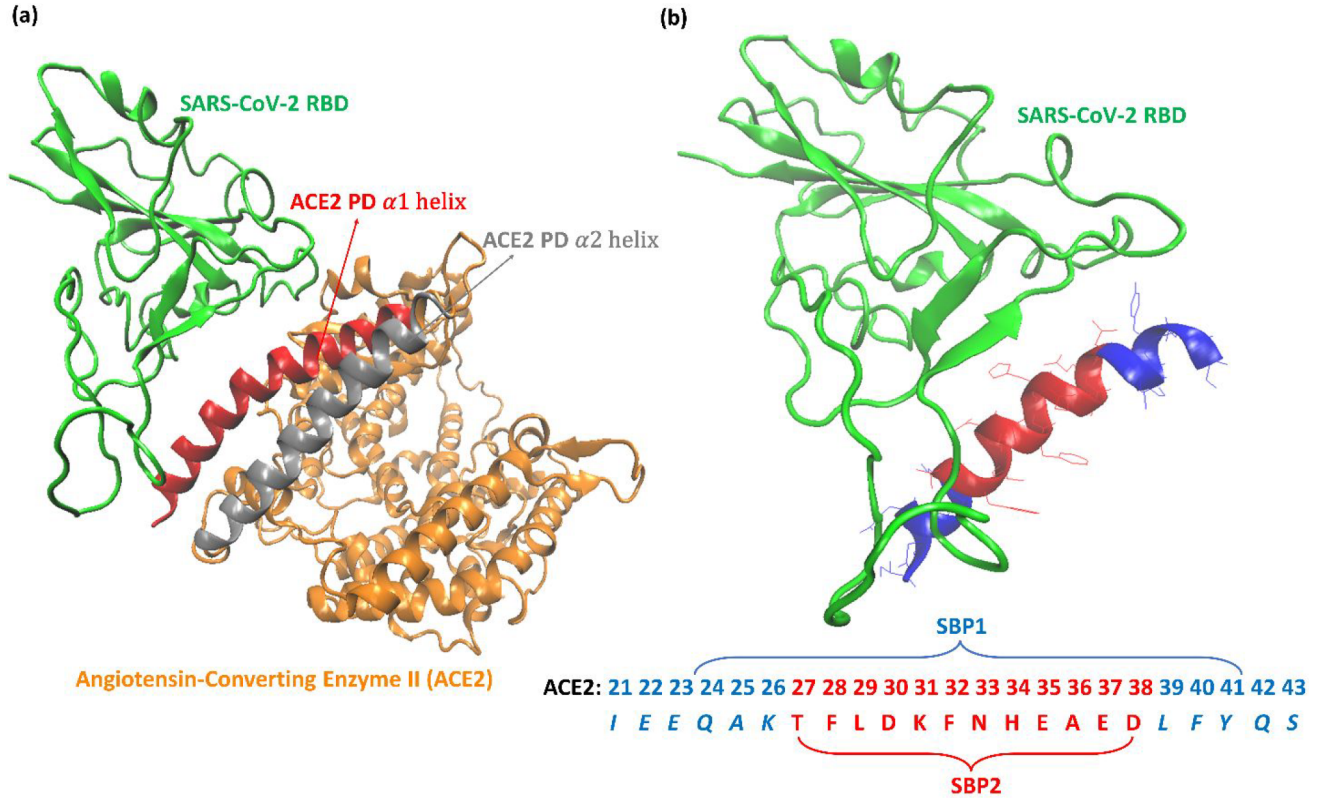

Figure 1. (a) The structure of the complex between SARS-CoV-2 and ACE2 (PDB ID: 6M17). This shows that the molecular recognition of ACE2 peptidase domain (orange) by SARS-CoV-2 receptor-binding domain (green) involves primarily the ACE2 α1 helix (red) with a minor contribution from the ACE2 α2 helix (gray). (b) Peptide sequence (*IEEQAK***TFLDKFNHEAED***LFYQS* for residue ID: 21−43, termed "SBP1") derived from ACE2 α1 helix was confirmed experimentally to have an affinity of ∼1.3 μM with SARS-CoV-2 RBD. However, the middle fragment, the peptide sequence (**TFLDKFNHEAED** for residue ID: 27−38, termed "SBP2") does not bind with SARS-CoV-2 RBD in similar experiments. In our in silico evolution algorithm, residues 27−38 (SBP2 domain of SBP1) were subjected to both sequence and conformation change moves while residues 21−26 (***IEEQAK***) and 39−43 (***LFYQS***) were subjected only to conformation change moves.

first been coated with recombinantly expressed ACE2. Plates were incubated overnight at 4 °C with gentle shaking. Solution with unbound SARS-CoV-2 RBD was removed by aspiration, and the plates were washed four times with 1× Wash Buffer to remove any loosely bound SARS-CoV-2 RBD. Horseradish peroxidase (HRP)-conjugated IgG, as supplied, was then added to the wells, and the plates were incubated for 1 h at 10 °C. The HRP-IgG solution was then removed by aspiration and the plates were washed four times with 1× Wash Buffer. The HRP substrate 3,3′,5,5′-tetramethylbenzidine (TMB) was then added to each well of the plate. After 30 min, the HRP-TMB reaction was stopped with 0.2 M sulfuric acid Stop Solution. The solution absorbance was then measured (λ = 450 nm) using a SpectraMax M5 plate-reader and Softmax Pro v5.0 software. In the commercial assay, HRP-conjugated IgG binds to the SARS-CoV-2 RBD protein and reacts with the TMB solution, producing a yellow color that is proportional to the amount of SARS-CoV-2 RBD bound to ACE2 adsorbed onto the plate. Peptide inhibition of ACE2:SARS-CoV-2 RBD binding leads to a decrease in formation of this yellow product, which can be measured as a decrease in absorbance relative to the control. Two independent replicates were performed per sample. Data were analyzed for statistically significant differences relative to the control (0 mM peptide) using ANOVA and post hoc unpaired *t* tests.

3. RESULTS AND DISCUSSION

3.1. Peptide Design Strategy to Discover Spike-RBD WT Binding Peptides. The PepBD design algorithm requires an input structure of the complex formed between an initial peptide sequence (reference peptide) and the target biomolecule, in order to start the peptide search process. We focus on a 23-mer peptide fragment, SBP1, residues 21−43 on the peptidase domain of the α1 helix on human ACE2, which is present at the binding interface of SARS-CoV-2 RBD WT. This structure is derived from the cryo-EM structure (PDB ID: 6M17) determined by Yan et al[5] of a full-length human ACE2-B^{0}AT1 complex bound to the SARS-CoV-2 RBD WT (Figure 1a,b). We perform 100 ns explicit-solvent MD simulations with the Amber18 software suite on four complexes: (i) peptide SBP1 (hACE2 amino acids 21−43, *IEEQAK***TFLDKFNHEAED***LFYQS*) with SARS-CoV-2 RBD WT, (ii) a truncated SBP1 lacking both N- and C-terminal flanking domains (hACE2 amino acids 27−38, SBP2, **TFLDKFNHEAED**) with RBD-WT, (iii) a truncated SBP1 lacking only the C-terminal flanking domain (hACE2 amino acids 21−38, *IEEQAK***TFLDKFNHEAED**) with SARS-CoV-2 RBD WT, and (iv) a truncated SBP1 lacking only the N-terminal flanking domain (hACE2 amino acids 27−43, **TFLDKFNHEAED***LFYQS*) with SARS-CoV-2 RBD WT. Full-length SBP1 and SARS-CoV-2 RBD WT (i.e., complex (i)) form stable contacts, whereas none of the truncated SBP1 variants ((ii) to (iv)) form stable complexes with SARS-CoV-2 RBD WT. The

https://doi.org/10.1021/acs.jpcb.2c03918
J. Phys. Chem. B 2022, 126, 8129−8139

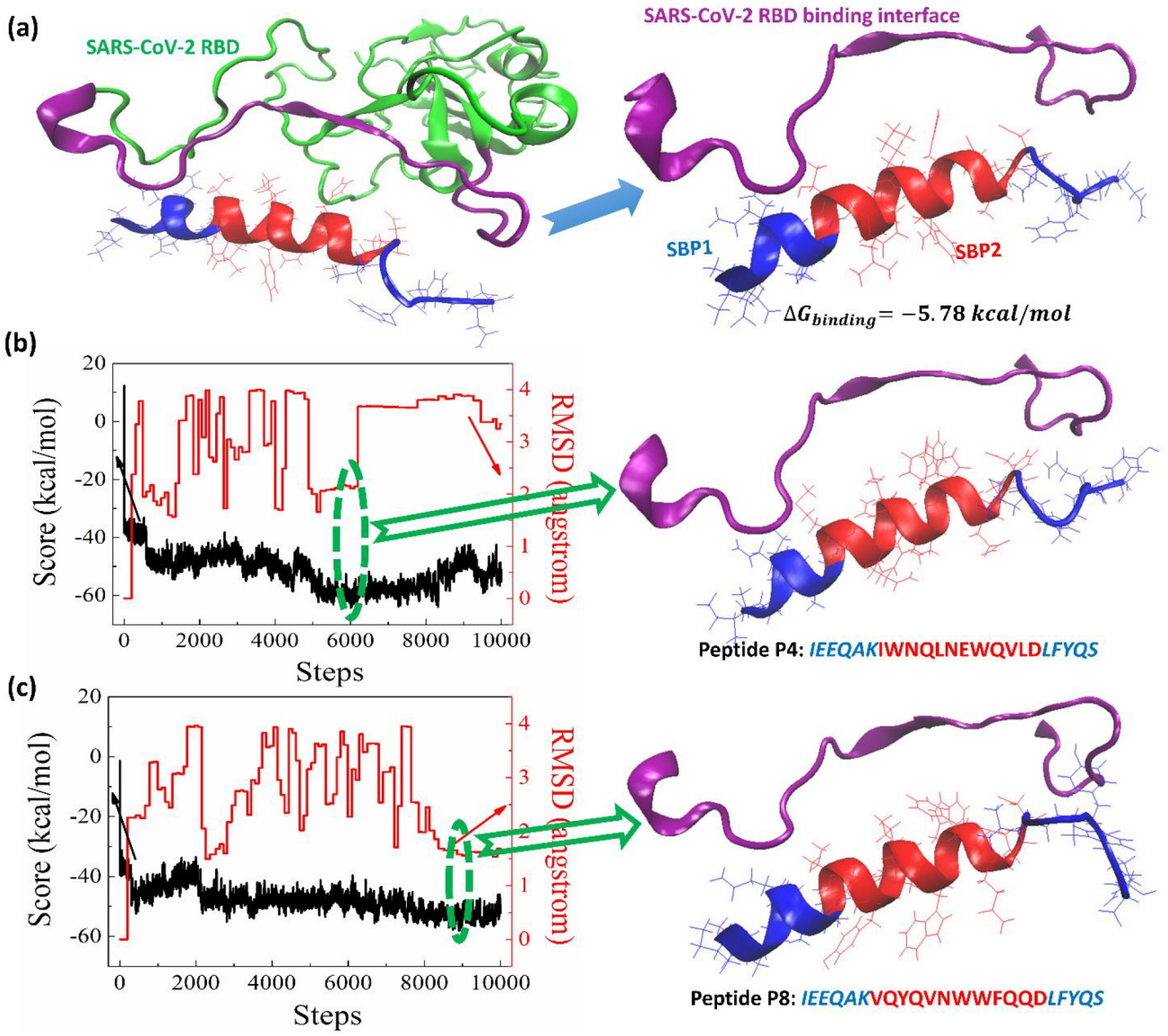

Figure 2. Computational modeling of peptide SBP1:SARS-CoV-2 RBD-WT complex and in silico peptide evolution. (a) Left side: Starting input structure of SBP1:SARS-CoV-2 RBD-WT for PepBD obtained after a 100 ns atomistic MD simulation of the complex between SARS-CoV-2 RBD-WT (in green) and SBP1 (in blue and red) obtained from PDB ID: 6M17. Right Side: SBP1 at the binding interface of the RBD (in purple). The score/RMSD vs sequence and conformation change steps for (b) Case One (left side) resulting in peptide P4 (right side) and for (c) Case Two (left side) resulting in peptide P8 (right side). The dotted ellipses (in green) and arrows (in green) correspond to the region on the score/RMSD profile of Cases 1 and 2, where peptides P4 and P8 are obtained, respectively.

binding free energy ($\Delta G_{binding}$) of the simulated full-length SBP1:SARS-CoV-2 RBD WT complex is predicted to be −5.78 kcal/mol. These simulations suggested that the N- and C-terminal flanking domains of SBP1 are important for SARS-CoV-2 RBD WT binding, consistent with a prior experimental report which showed that SBP1 binds SARS-CoV-2 RBD WT with low micromolar affinity, whereas the truncated SBP2 variant lacking both the N- and C-terminal flanking domains had no measurable binding affinity.[12,13] Hence, full-length SBP1 is chosen as our reference peptide and the simulated complex of SBP1:SARS-CoV-2 RBD WT is used as the starting input structure for PepBD (Figure 2a).

Next, we specify the hydration properties for the designed peptides as input parameters in the PepBD algorithm. Since the N and C termini proved to be important in the binding of SBP1 and RBD WT, we decided to mutate only the residues within the central SBP2 domain of SBP1 during the PepBD iterations, while allowing conformation change moves within the entire SBP1 peptide. The SBP2 region (**TFLDKFNHEAED**) has 12 residues: 3 hydrophobic residues (2 Phe-F, 1 Leu-L), 3 hydrophilic residues (1 Thr-T, 1 Asn-N, 1 His-H), four negatively charged residues (2 Asp-D, 2 Glu-E), 1 positively charged residue (1 Lys-K), 1 other residue (1 Ala-A), and no glycine residue. The number of hydrophobic and hydrophilic amino acids on our designed peptide chain of SBP2 was chosen to be greater than the numbers on SBP2, as hydrophobic residues tend to favor specificity in the binding behavior, while hydrophilic residues contribute to peptide solubility. Analysis of the residues present on the binding interface of SARS-CoV-2 RBD WT reveals that it has a high concentration of positively charged residues. Hence, we chose to allow negatively charged residues but avoid positively

https://doi.org/10.1021/acs.jpcb.2c03918
J. Phys. Chem. B 2022, 126, 8129−8139

Table 1. Γ_{score} (kcal/mol) Obtained from the PepBD Algorithm, $\Delta G^{avg}_{binding}$ (kcal/mol) Obtained by Averaging over Three Independent 100 ns Explicit Solvent MD Simulation Runs and Intrinsic Solubility Scores for Peptides Binding to the SARS-CoV-2 RBD-WT by the CamSol Method

peptide	sequences	Γ_{score} (kcal/mol)	$\Delta G^{avg}_{binding}$(kcal/mol)	intrinsic solubility score
SBP1	*IEEQAK***TFLDKFNHEAED***LFYQS*		−5.78	1.74
SBP2	**TFLDKFNHEAED**		0.00	
Case 1				
P3	*IEEQAK***IWNFVQEWFQHD***LFYQS*	−64.49	−11.85	0.55
P4	*IEEQAK***IWNQLNEWQVLD***LFYQS*	−64.26	−7.31	1.07
P5	*IEEQAK***MWNQLLEWQNLD***LFYQS*	−64.13	−11.99	1.34
P6	*IEEQAK***MTQQIYEWWQWD***LFYQS*	−60.49	−16.20	0.25
P7	*IEEQAK***ITQQLLEWWSWD***LFYQS*	−60.18	−6.72	0.43
Case 2				
P8	*IEEQAK***VQYQVNWWFQQD***LFYQS*	−56.52	−11.60	−0.32
P9	*IEEQAK***MTVQQNIWFNLD***LFYQS*	−55.19	−16.53	0.11
P10	*IEEQAK***IVVQVQHWFNQD***LFYQS*	−53.23	−9.83	0.25
P11	*IEEQAK***MIQMINHWFNQD***LFYQS*	−41.85	−13.16	0.84
P12	*IEEQAK***LSMMINHWWQQD***LFYQS*	−41.57	−7.70	0.81

charged residues on the designed peptide chain of SBP2 as the negatively charged residues will contribute to favorable electrostatic interactions. We investigate two cases with two different sets of hydration properties for the peptide chain: Case One: $N_{hydrophobic}$ = 6, $N_{hydrophilic}$ = 4, $N_{positive\ charge}$ = 0, $N_{negative\ charge}$ = 2, N_{other} = 0, and $N_{glycine}$ = 0; and Case Two: $N_{hydrophobic}$ = 6, $N_{hydrophilic}$ = 5, $N_{positive\ charge}$ = 0, $N_{negative\ charge}$ = 1, N_{other} = 0, and $N_{glycine}$ = 0.

3.2. In Silico Evolution of SARS-CoV-2 RBD WT Binding Peptides. Starting with the input structure of the SBP1:SARS-CoV-2 RBD WT complex described in Figure 2a, we perform eight independent sequence evolutions: Cases One and Two (each starting from three different random seeds plus a fourth search that samples only sequence change moves). This is done to ensure that the computational algorithm samples peptides from a large pool of peptide sequences and conformations. All eight evolutions are initialized with random sequences and then proceed along different search pathways that are determined by their specific input parameters. Overall, the algorithm sampled approximately 450000 distinct peptide sequences from a pool of $\sim 10^{13}$ possible peptide candidates (see calculation of the number of theoretically possible peptide sequences in Cases 1 and 2 in the Supporting Information). Our PepBD algorithm efficiently samples high affinity peptides to the RBD evaluated using the score function (Γ_{score}). Figure 2b shows an example of the score/RMSD vs the number of steps for Case One, as well as the peptide P4:SARS-CoV-2 RBD WT binding interface structure that is obtained from that evolution. The score/RMSD vs the number of steps for one of the Case Two evolutions and the peptide P8:SARS-CoV-2 RBD WT binding interface structure obtained from that evolution are shown in Figure 2c.

Explicit-solvent atomistic MD simulations are carried out for 100 ns to examine the dynamic properties of the top peptide candidates with the lowest scores when bound to the Spike-RBD WT. The score and the binding free energies of the initial peptide SBP1 and the top 10 peptide candidates (P3−P12) are reported in Table 1 (Note: the lower the value of $\Delta G_{binding}$, the higher the binding affinity). All of the peptides listed in Table 1 have binding free energies that are lower than SBP1, suggesting that these in silico peptides bind to RBD with higher affinity than SBP1. It is to be noted that some inconsistency is expected between $\Delta G^{avg}_{binding}$ and the corresponding K_D values determined from experiments. This is because the MM/GBSA approach used to analyze the explicit solvent molecular dynamics trajectories and evaluate the $\Delta G^{avg}_{binding}$ is an implicit solvent method and partly neglects the effect of water. Hence, it does not account for the true enthalpy and entropy of desolvation of both the SARS-CoV-2 RBD and the peptide ligand upon binding. The enthalpy and entropy of desolvation are considered via the dielectric constant of the solvent and are expected to only partially account for the free energy of desolvation. Furthermore, the one-average MM/GBSA (1A-MM/GBSA) approach as used here neglects the change in structure of the peptide and receptor upon peptide binding and, thus, considers the structure of the peptide and receptor to be identical in the bound and unbound states.[28−30] The values of $\Delta G^{avg}_{binding}$ are instead a useful tool to guide the selection of sequence variants for experimental characterization. Table 1 also lists the solubility scores of the peptides, which are calculated using the CamSol method (http://www-cohsoftware.ch.cam.ac.uk). The CamSol method was developed in the Vendruscolo lab[31,32] and is a sequence-based approach for predicting protein/peptide solubility. In the CAMSol method, highly soluble residues in a protein or peptide are predicted to have intrinsic residue solubility scores close to or larger than 1, while residues with scores close to or less than −1 are poorly soluble.

3.3. Experimental Evaluation of the SARS-CoV-2 RBD Binding Properties of PepBD-Designed Peptides. To optimize the experimental cost, time, and efficiency we evaluated the binding properties of seven peptides (P4, P5, P6, P9, P10, P11, and P12) to the SARS-CoV-2 RBD-WT. These peptides were chosen based on their favorable in silico $\Delta G^{avg}_{binding}$ values and intrinsic solubility scores as predicted by the CAMSol method. Peptides P6 and P9 could not be synthesized, and peptide P11 was only soluble under very alkaline conditions (pH > 11) or at concentrations that were too low to be accurately measured in tryptophan fluorescence quenching experiments. Peptide P7 was excluded, as it has a less favorable binding free energy than the other peptides. Peptides P3 and P8 were not considered as their $\Delta G^{avg}_{binding}$ values were similar to that of peptide P5, so we did not expect significant difference in their binding affinity to the SARS-CoV-2 RBD. Another reason that peptide P8 was excluded was that its intrinsic solubility score, −0.32, was low.

https://doi.org/10.1021/acs.jpcb.2c03918
J. Phys. Chem. B 2022, 126, 8129−8139

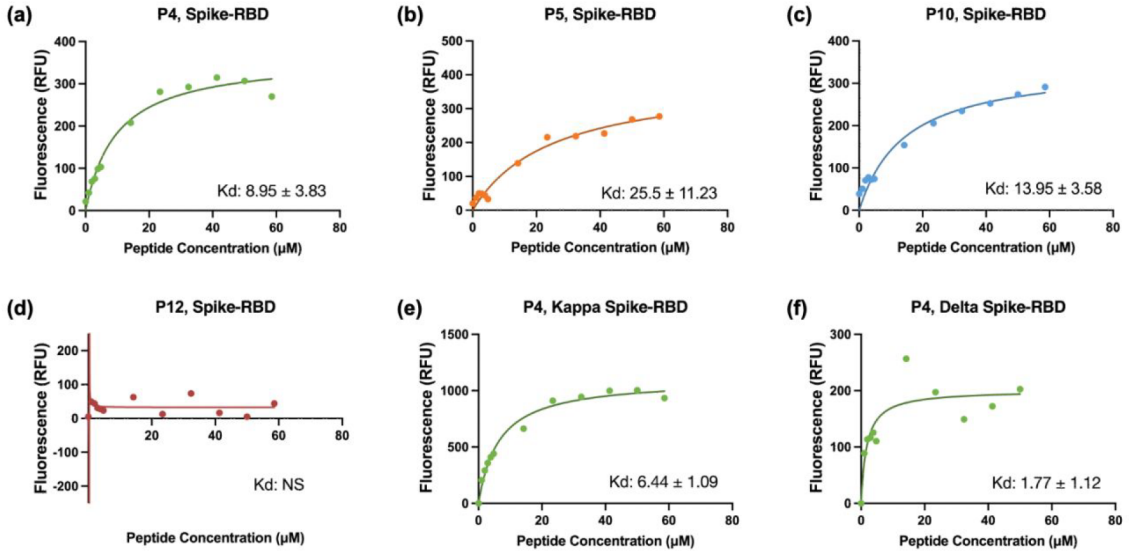

Figure 3. Tryptophan fluorescence quenching measurements of the solution-phase binding of ACE2 SBP1 mutants to SARS-CoV-2 Spike proteins. ΔRFU plots of aqueous solutions: of SARS-CoV-2 SARS-CoV-2 RBD with (a) P4, (b) P5, (c) P10, and (d) P12; of κ SARS-CoV-2 RBD with (e) P4; and of δ SARS-CoV-2 RBD with (f) P4. All data are reported as mean ± standard deviation. Disassociation constants (K_d) are reported in μM (experimental replicates, n = 3 for b, c, e, and f; n = 2 for d).

To experimentally evaluate the binding of PepBD-designed peptides to SARS-CoV-2 RBD-WT, we first used tryptophan fluorescence quenching of samples containing a fixed amount of SARS-CoV-2 RBD WT with increasing amounts of peptide to estimate the solution-phase binding affinity. Such solution-phase binding assays provide an approximate measure of the strength of the solution-phase interaction between each peptide and SARS-CoV-2 RBD WT. Solution-phase binding assays also avoid artifacts that can arise from immobilization of the peptide inhibitor or SARS-CoV-2 RBD WT.[33] In the solution phase assay used here, an increase in tryptophan fluorescence quenching (i.e., ΔRFU) indicated binding of a peptide to SARS-CoV-2 RBD WT. Peptides P4, P5, P10, and P12 each had at least one tryptophan residue, (2, 2, 1, and 2, respectively), whereas SBP1 has no tryptophan residues and was therefore not suitable for this assay. The PepBD-designed peptides and the SARS-CoV-2 RBD protein both have tryptophan residues that independently fluoresce. Thus, the results of these solution-phase binding assays are reported using the change in Relative Fluorescence Units (ΔRFU) between the predicted and experimental fluorescence emission as described in the methods.

ΔRFU increased with peptide concentration for samples containing P4, P5, and P10, indicating that these peptides bound to SARS-CoV-2 RBD (Figure 3a–c). In contrast, ΔRFU did not change from baseline for samples containing P12 (Figure 3d), suggesting that this peptide was unable to bind to SARS-CoV-2 RBD WT. Nonlinear regression using a single-site binding model of the ΔRFU values relative to peptide concentration for P4, P5, and P10, estimated that the peptides bound SARS-CoV-2 RBD with micromolar dissociation constants (see Supporting Information, Table S2). This was consistent with a prior report that estimated a dissociation constant for SBP1:RBD-WT binding of 1.3 μM using biolayer interferometry.[13] We note that surface immobilization and transport effects can lead to discrepancies between biolayer interferometry and solution-phase binding measurements, which complicates comparison of dissociation constants measured using different techniques.[33] Figure 3e,f shows the tryptophan fluorescence quenching measurements of P4 bound to κ and δ strains of SARS-CoV-2 RBD (explained later in section 3.5).

Based on the solution-phase binding data, we assessed the relative activity of SBP1, P4, P5, and P10 to competitively inhibit ACE2 and SARS-CoV-2 RBD WT binding using an ELISA assay that measures the amount of SARS-CoV-2 RBD WT captured by immobilized ACE2. In this assay, a decrease in measured optical density below the SARS-CoV-2 RBD WT control would indicate that the peptide is inhibiting ACE2:SARS-CoV-2 RBD WT binding. All peptides (SBP1, P4, P5, and P10) failed to inhibit ACE2:SARS-CoV-2 RBD WT binding up to a concentration of 50 μM (Figure 4). Unexpectedly, peptide P10 increased the measured optical density above the control with increasing peptide concen-

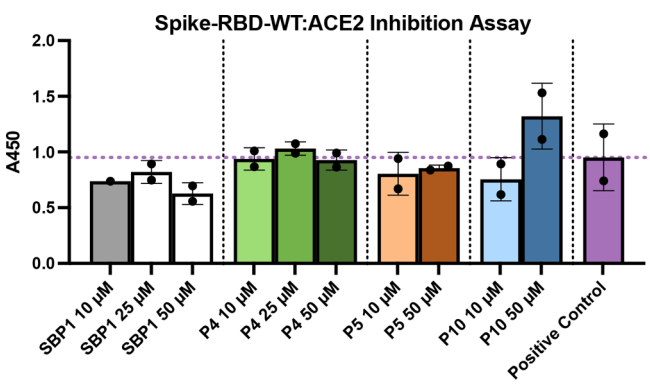

Figure 4. Measurement of the inhibition of SARS-CoV-2 RBD-ACE2 interaction in the presence of ACE2 SBP1 mutants. Optical density at 450 nm correlates to the amount of SARS-CoV-2 RBD bound to surface-adsorbed ACE-2 as a function of inhibitor concentration in solution. Results of the competitive COVID-19 Spike-ACE2 binding assay show a lack of inhibitory function of SBP1, P4, P5, and P10. All data are reported as mean ± standard deviation. (μM = 10–50, n = 2).

https://doi.org/10.1021/acs.jpcb.2c03918
J. Phys. Chem. B 2022, 126, 8129–8139

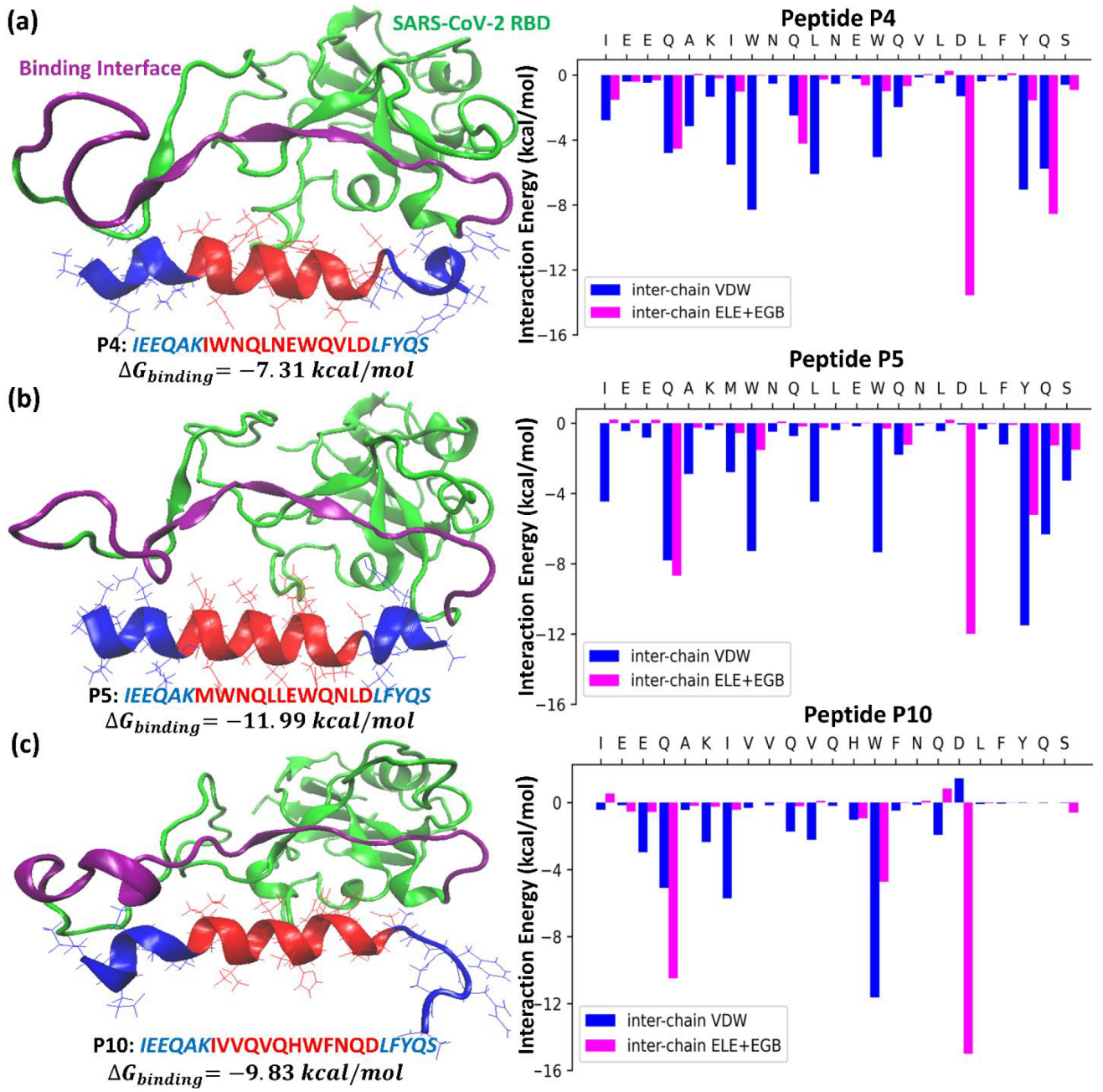

Figure 5. Snapshots of the representative structure of (a) P4 bound to SARS-CoV-2 RBD-WT, (b) P5 bound to SARS-CoV-2 RBD-WT, and (c) P10 bound to SARS-CoV-2 RBD-WT after 100 ns atomistic simulation (left side). The SARS-CoV-2 RBD-WT is represented by the green ribbon; the peptide (residues 21−26 and 39−43) is in blue and the SBP2 domain (residues 27−38) is in red. The residues along the binding interface on the SARS-CoV-2 RBD are shown in purple. The various contributions to the binding energy along the peptide chain for the three structures are shown in the adjacent plots (right side).

tration. Control measurements of P10 at a range of concentrations or in the absence of SARS-CoV-2 RBD WT also showed an increase in optical density. This demonstrates that P10 binds to other components of this assay, such as the plate-bound ACE2, leading to erroneous signal generation. Thus, P10 is not specific for SARS-CoV-2 RBD (see Supporting Information, Figure S1). Collectively, these results demonstrate that the P4 and P5 peptides designed by the PepBD algorithm can bind to RBD WT but cannot competitively inhibit ACE2:RBD WT binding, analogous to the behavior of the parent SBP1 peptide.

3.4. Computational Analysis of P4, P5, and P10 Binding to SARS-CoV-2 RBD WT. To understand the observed differences in binding affinity and inhibitory potency of P4, P5, and P10 to SARS-CoV-2 RBD WT, we study the contributions by the individual residues of each peptide to the interaction energy (Figure 5a−c, right side). We also construct energy panels detailing the pair wise VDW and ELE+EGB interactions of P4, P5 and P10 bound to SARS-CoV-2 RBD WT (see Supporting Information, Figure S2). D (Asp, negatively charged) at the 18th position is the most significant contributor to the binding affinity of all three peptides, as it formed strong ionic bonds with 403R (Arg, positively charged)

https://doi.org/10.1021/acs.jpcb.2c03918
J. Phys. Chem. B 2022, 126, 8129−8139

of the RBD. Notably, SBP1 also has a D (Asp) at the 18th position, and we allow the 18th position to be mutated in the PepBD screening process. The retention of D in the 18th position after PepBD screening demonstrates the ability of our algorithm to predict the optimal residues for robust intermolecular contacts. W (Trp, aromatic hydrophobic) at the 14th position in P4, P5, and P10, and again in the eighth position in P4 and P5, contribute to the binding affinity via $\pi-\pi$ stacking, cation$-\pi$, or anion$-\pi$ interactions, and VDW contacts. Notably, the aliphatic hydrophobic residue V (Val) at the eighth position in P10 does not contribute significantly to the binding affinity, underscoring the importance of having an aromatic residue at this position (F in SBP1 and W in P4/P5, respectively) for increased binding affinity. The N-terminal flanking region of SBP1, which is not mutated by PepBD, also contributes to the binding affinity. In particular, Q (Gln) at the fourth position on SBP1 and on all of the designed peptides interacts strongly with RBD-WT via both VDW and ELE +EGB interactions. Simulations also predict that the helical structure of the C-terminal flanking residues (residues 19−23), which are also not mutated by PepBD, is maintained in the bound state of peptide P4 (Figure 5a, left side) and P5 (Figure 5b, left side), whereas P10 (Figure 5c, left side) adopts a random-coil structure in this region. Contacts between Y (Try) and Q (Gln) in this region on the peptides with SARS-CoV-2 RBD WT contribute to the binding affinity; however, the Q residue in P4 is predicted to contribute more energy from ELE +EGB interactions than the same residue in P5.

3.5. Binding Properties of SBP1 and P4 Against the RBD of Other SARS-CoV-2 Strains. As the pandemic progressed, new and more virulent strains of SARS-CoV-2 such as the Alpha-B.1.1.7, Beta-B.1.351, Gamma-P.1, Kappa-B.1.617.1, Delta-B.1.617.2, and Omicron-B.1.1.529 variants emerged. More information about the mutations in the RBD of the various SARS-CoV-2 strains is provided in the Supporting Information. Hence, we decided to perform 100 ns MD simulations of P4 and our reference peptide SBP1 to check their binding affinity against SARS-CoV-2 RBD across all the variants (summarized in Table 2). The $\Delta G^{avg}_{binding}$ values indicate that P4 has stronger binding affinity than SBP1 against the SARS-CoV-2 RBD of all the variants except the Alpha variant. These simulation results indicate that our in silico designed peptide P4 may recognize new strains that emerge as the COVID-19 pandemic progresses more effectively than SBP1.

Table 2. $\Delta G^{avg}_{binding}$ values of SBP1 and P4 Bound to SARS-CoV-2-RBD of Alpha, Beta, Gamma, Kappa, Delta, and Omicron Variant Averaged over Three Independent 100 ns Explicit Solvent MD Simulation Runs

	$\Delta G^{avg}_{binding}$(kcal/mol)	
SARS-CoV-2 variant	SBP1	P4
Wuhan-Hu-1 (WT)	−5.78	−11.85
Alpha	−2.18	−0.57
Beta	−3.21	−14.74
Gamma	−2.03	−14.83
Kappa	−5.88	−10.98
Delta	−10.02	−15.22
Omicron	−0.83	−17.05

In light of these predictions, we experimentally measured the solution-phase binding of P4 and P5 to both δ SARS-CoV-2 RBD and κ SARS-CoV-2 RBD (Figure 3e,f). P4 binds to both δ SARS-CoV-2 RBD and κ SARS-CoV-2 RBD with micromolar solution-phase dissociation constants that were comparable to that of P4:SARS-CoV-2 RBD binding. P5 also binds to κ SARS-CoV-2 RBD, with a micromolar solution-phase dissociation constant as measured via tryptophan fluorescence quenching (see Supporting Information, Figure S3). Collectively, these data demonstrate that PepBD and molecular dynamics simulations can be used to identify ACE2 variants that bind to emergent SARS-CoV-2 Spike RBD variants.

4. CONCLUSION

The goal of this study was to evaluate the use of the PepBD algorithm to generate mutated variants of the ACE2-derived SBP1 peptide that demonstrate increased potency for inhibiting ACE2:SARS-CoV-2 RBD binding. Using this in silico approach, 10 peptides were identified that were predicted to have a lower binding free energy than SBP1. Five of these peptides were evaluated experimentally of which three bind to RBD WT in solution with micromolar dissociation constants, one does not bind, and one is insoluble. Peptides 4 and 5 also bind to the δ SARS-CoV-2 RBD and κ SARS-CoV-2 RBD with micromolar dissociation constants, suggesting the potential of our approach to identify peptides that recognize emergent SARS-CoV-2 variants. However, neither SBP1 nor the designed peptides could inhibit ACE2:SARS-CoV-2 RBD binding in a competitive ELISA assay, suggesting that relatively short peptides with modest binding affinity are incapable of outcompeting high-affinity RBD:ACE2 interactions.

Increasing binding affinity by extending the length of the peptide or achieving native-like peptide secondary structures could lead to effective inhibitors, as has been shown with ACE2 mutants and designed mini-proteins.[9,34]

Collectively, our results demonstrate the potential of the PepBD algorithm to identify peptide-based molecules that can recognize the SARS-CoV-2 Spike protein or molecular components of other emerging pathogens.

■ ASSOCIATED CONTENT

Supporting Information

The Supporting Information is available free of charge at https://pubs.acs.org/doi/10.1021/acs.jpcb.2c03918.

Classification of the 20 natural amino acids into six residue type (Table S1); Results of nonlinear regression for for tryptophan fluorescence quenching measurements of the solution-phase binding of ACE2 SBP1 mutant peptides P4, P5, P10, and P12 to SARS-CoV-2 spike proteins (Table S2); Measurement of the inhibition of SARS-CoV-2 RBD-ACE2 interaction in the presence of ACE2 SBP1 mutant P10 at varying concentrations (Figure S1); Energy panels detailing the pairwise interactions of P4, P5, and P10 with SARS-CoV-2 RBD (Figure S2); Tryptophan fluorescence quenching measurement of the solution-phase binding of peptide P5 to κ SARS-CoV-2 Spike protein (Figure S3); Structure of SARS-CoV-RBD of Alpha, Beta, Gamma, Kappa, Delta, and Omicron variant (Figures S4 and S5); Snapshots of the representative structure of P4 bound to the Alpha, Beta, Gamma, Kappa, Delta, and Omicron variants (Figure S6); Calculation of the number of theoretically possible peptide sequences in Cases 1 and 2 (PDF)

https://doi.org/10.1021/acs.jpcb.2c03918
J. Phys. Chem. B 2022, 126, 8129−8139

AUTHOR INFORMATION

Corresponding Author

Carol K. Hall − *Department of Chemical and Biomolecular Engineering, North Carolina State University, Raleigh, North Carolina 27695-7905, United States;* orcid.org/0000-0002-7425-587X; Email: hall@ncsu.edu

Authors

Sudeep Sarma − *Department of Chemical and Biomolecular Engineering, North Carolina State University, Raleigh, North Carolina 27695-7905, United States;* orcid.org/0000-0002-4642-7689

Stephanie M. Herrera − *J. Crayton Pruitt Family Department of Biomedical Engineering, University of Florida, Gainesville, Florida 32611, United States*

Xingqing Xiao − *Department of Chemical and Biomolecular Engineering, North Carolina State University, Raleigh, North Carolina 27695-7905, United States;* orcid.org/0000-0003-3462-3049

Gregory A. Hudalla − *J. Crayton Pruitt Family Department of Biomedical Engineering, University of Florida, Gainesville, Florida 32611, United States*

Complete contact information is available at: https://pubs.acs.org/10.1021/acs.jpcb.2c03918

Author Contributions

#These authors (S.S. and S.M.H.) contributed equally to this work and should be considered co-first authors.

Notes

The authors declare no competing financial interest.

ACKNOWLEDGMENTS

This research was supported by funds from the National Science Foundation (Grant CBET-1743432). This work used the Extreme Science and Engineering Discovery Environment (XSEDE), supported by National Science Foundation (ACI-1548562). S.S., X.X., and C.K.H. thank the San Diego Supercomputer Center (SDSC) for computing time.

REFERENCES

(1) World Health OrganizationWeekly epidemiological update on COVID-19; Available from: https://www.who.int/emergencies/diseases/novel-coronavirus-2019/situation-reports.

(2) World Health OrganizationTracking SARS-CoV-2 variants; Available from: https://www.who.int/en/activities/tracking-SARS-CoV-2-variants/.

(3) Sah, P.; Vilches, T. N.; Moghadas, S. M.; Fitzpatrick, M. C.; Singer, B. H.; Hotez, P. J.; Galvani, A. P. Accelerated vaccine rollout is imperative to mitigate highly transmissible COVID-19 variants. *EClinicalMedicine* **2021**, *35*, 100865.

(4) Zhu, N.; Zhang, D.; Wang, W.; Li, X.; Yang, B.; Song, J.; Zhao, X.; Huang, B.; Shi, W.; Lu, R.; et al. A Novel Coronavirus from Patients with Pneumonia in China, 2019. *N. Engl. J. Med.* **2020**, *382* (8), 727−733.

(5) Zhou, P.; Yang, X. L.; Wang, X. G.; Hu, B.; Zhang, L.; Zhang, W.; Si, H. R.; Zhu, Y.; Li, B.; Huang, C. L.; et al. A pneumonia outbreak associated with a new coronavirus of probable bat origin. *Nature* **2020**, *579*, 270−273.

(6) Wrapp, D.; Wang, N.; Corbett, K. S.; Goldsmith, J. A.; Hsieh, C. L.; Abiona, O.; Graham, B. S.; McLellan, J. S. Cryo-EM structure of the 2019-nCoV spike in the prefusion conformation. *Science* **2020**, *367*, 1260−1263.

(7) Yan, R.; Zhang, Y.; Li, Y.; Xia, L.; Guo, Y.; Zhou, Q. Structural basis for the recognition of SARS-CoV-2 by full-length human ACE2. *Science* **2020**, *367*, 1444−1448.

(8) Kirchdoerfer, R. N.; Wang, N.; Pallesen, J.; Wrapp, D.; Turner, H. L.; Cottrell, C. A.; Corbett, K. S.; Graham, B. S.; McLellan, J. S.; Ward, A. B. Stabilized coronavirus spikes are resistant to conformational changes induced by receptor recognition or proteolysis. *Sci. Rep.* **2018**, *8*, 1−11.

(9) Chan, K. K.; Dorosky, D.; Sharma, P.; Abbasi, S. A.; Dye, J. M.; Kranz, D. M.; Herbert, A. S.; Procko, E.; et al. Engineering human ACE2 to optimize binding to the spike protein of SARS coronavirus 2. *Science* **2020**, *369*, 1261−1265.

(10) Han, Y.; Král, P.; et al. Computational Design of ACE2-Based Peptide Inhibitors of SARS-CoV-2. *ACS Nano* **2020**, *14* (4), 5143−5147.

(11) Han, D. P.; Penn-Nicholson, A.; Cho, M. W. Identification of Critical Determinants on ACE2 for SARS-CoV- Entry and Development of a Potent Entry Inhibitor. *Virology* **2006**, *350* (1), 15−25.

(12) Zhang, G.; Pomplun, S.; Loftis, A. R.; Tan, X.; Loas, A.; Pentelute, B. L. The first-in-class peptide binder to the SARS-COV-2 spike protein. *bioRxiv 2020.03.19.999318* **2020**, na.

(13) Zhang, G.; Pomplun, S.; Loftis, A. R.; Tan, X.; Loas, A.; Pentelute, B. L. Investigation of ACE2 N-terminal fragments binding to SARS-COV-2 Spike RBD. *bioRxiv 2020.03.19.999318* **2020**, na.

(14) Pomplun, S.; Jbara, M.; Quartararo, A. J.; Zhang, G.; Brown, J. S.; Lee, Y. C.; Ye, X.; Hanna, S.; Pentelute, B. L. De Novo Discovery of High-Affinity Peptide Binders for the SARS-CoV–2 Spike Protein. *ACS Cent. Sci.* **2021**, *7*, 156−163.

(15) Xiao, X.; Hall, C. K.; Agris, P. F. The design of a peptide sequence to inhibit HIV replication: a search algorithm combining Monte Carlo and self-consistent mean field techniques. *J. Biomol. Struct. Dyn.* **2014**, *32*, 1523−1536.

(16) Xiao, X.; Agris, P. F.; Hall, C. K. Introducing folding stability into the score function for computational design of RNA-binding peptides boosts the probability of success. *Proteins* **2016**, *84*, 700−711.

(17) Xiao, X.; Agris, P. F.; Hall, C. K. Designing peptide sequences in flexible chain conformations to bind RNA using Monte Carlo, self consistent mean field, and concerted rotation techniques. *J. Chem. Theory Comput.* **2015**, *11*, 740−752.

(18) Xiao, X.; Hung, M. E.; Leonard, J. N.; Hall, C. K. Adding energy minimization strategy to peptide-design algorithm enables better search for RNA-binding peptides: Redesigned λ N peptide binds boxB RNA. *J. Comput. Chem.* **2016**, *37*, 2423−2435.

(19) Xiao, X.; Wang, Y.; Leonard, J. N.; Hall, C. K. Extended Concerted Rotation Technique Enhances the Sampling Efficiency of Computational Peptide-Design Algorithm. *J. Chem. Theory Comput.* **2017**, *13*, 5709−5720.

(20) Xiao, X.; Zhao, B.; Agris, P. F.; Hall, C. K. Simulation study of the ability of a computationally designed peptide to recognize target $tRNA^{Lys3}$ and other decoy tRNAs. *Protein Sci.* **2016**, *25*, 2243−2255.

(21) Spears, J. L.; Xiao, X.; Hall, C. K.; Agris, P. F. Amino acid signature enables proteins to recognize modified tRNA. *Biochemistry* **2014**, *53*, 1125−1133.

(22) Xiao, X.; Kuang, Z.; Slocik, J. M.; Tadepalli, S.; Brothers, M.; Kim, S.; Mirau, P. A.; Butkus, C.; Farmer, B. L.; Singamaneni, S.; et al. Advancing peptide-based biorecognition elements for biosensors using in-silico evolution. *ACS Sens.* **2018**, *3*, 1024−1031.

(23) Xiao, X.; et al. In Silico Discovery and Validation of Neuropeptide-Y-Binding Peptides for Sensors. *J. Phys. Chem. B* **2020**, *124*, 61−68.

(24) Reese, H. R.; Xiao, X.; Shanahan, C. C.; Chu, W.; Van Den Driessche, G. A.; Fourches, D.; Carbonell, R. G.; Hall, C. K.; Menegatti, S. Novel peptide ligands for antibody purification provide superior clearance of host cell protein impurities. *J. Chromatogr. A* **2020**, *1625*, 461237.

(25) Xiao, X.; Kilgore, R.; Sarma, S.; Chu, W.; Menegatti, S.; Hall, C. K. De novo discovery of peptide-based affinity ligands for the Fab

fragment of human immunoglobulin G. *J. Chromatogr. A* **2022**, *1669*, 462941−15.
(26) Xiao, X.; Sarma, S.; Menegatti, S.; Crook, N.; Magness, S. T.; Hall, C. K. *In-silico* identification of experimental validation of peptide-based inhibitors targeting *Clostridium difficile* toxin A. *ACS Chem. Biol.* **2022**, *17*, 118−128.
(27) Farhadi, S. A.; Bracho-Sanchez, E.; Fettis, M. M.; Seroski, D. T.; Freeman, S. L.; Restuccia, A.; Keselowsky, B. G.; Hudalla, G. A. Locally anchoring enzymes to tissues via extracellular glycan recognition. *Nat. Commun.* **2018**, *9*, 4943.
(28) Ryde, U.; Genheden, S. Comparison of end-point continuum-solvation methods for the calculation of protein-ligand binding free energies. *Proteins.* **2012**, *80*, 1326−1342.
(29) Ryde, U.; Genheden, S. The MM/PBSA and MM/GBSA methods to estimate ligand-binding affinities. *Expert Opin. Drug Discovery* **2015**, *10* (5), 449−461.
(30) Wang, E.; Sun, H.; Wang, J.; Wang, Z.; Liu, H.; Zhang, J. Z. H.; Hou, T. End-Point Binding Free Energy Calculation with MM/PBSA and MM/GBSA: Strategies and Applications in Drug Design. *Chem. Rev.* **2019**, *119*, 9478−9508.
(31) Sormanni, P.; Aprile, F. A.; Vendruscolo, M. The CamSol Method of Rational Design of Protein Mutants with Enhanced Solubility. *J. Mol. Biol.* **2015**, *427*, 478−490.
(32) Sormanni, P.; Amery, L.; Ekizoglou, S.; Vendruscolo, M.; Popovic, B. Rapid and accurate *in silico* solubility screening of a monoclonal antibody library. *Sci. Rep.* **2017**, *7*, 8200.
(33) Daniel, C.; Roupioz, Y.; Gasparutto, D.; Livache, T.; Buhot, A.; et al. Solution-phase vs surface-phase aptamer-protein affinity from a label-free kinetic biosensor. *PloS One* **2013**, *8*, No. e75419.
(34) Cao, L.; Goreshnik, I.; Coventry, B.; Case, J. B.; Miller, L.; Kozodoy, L.; Chen, R. E.; Carter, L.; Walls, A. C.; Park, Y. J.; et al. De novo design of picomolar SARS-CoV-2 miniprotein inhibitors. *Science* **2020**, *370*, 426−431.

https://doi.org/10.1021/acs.jpcb.2c03918
J. Phys. Chem. B 2022, 126, 8129−8139